Effects of differential mobility on biased diffusion of two species

2003 J. Phys. A: Math. Gen. 36 4963

(http://iopscience.iop.org/0305-4470/36/18/302)

INSTITUTE OF PHYSICS PUBLISHING JOURNAL OF PHYSICS A: MATHEMATICAL AND GENERAL

J. Phys. A: Math. Gen. **36** (2003) 4963–4975 PII: S0305-4470(03)59586-5

Effects of differential mobility on biased diffusion of two species

R S Hipolito, R K P Zia and B Schmittmann

Physics Department, Center for Stochastic Processes in Science and Engineering, Virginia Polytechnic Institute and State University, Blacksburg, VA 24061-0435, USA

Received 13 February 2003
Published 23 April 2003
Online at stacks.iop.org/JPhysA/36/4963

Abstract

Using simulations and a simple mean-field theory, we investigate jamming transitions in a two-species lattice gas under non-equilibrium steady-state conditions. The two types of particles diffuse with different mobilities on a square lattice, subject to an excluded volume constraint and biased in opposite directions. Varying filling fraction, differential mobility and drive, we map out the phase diagram, identifying first order and continuous transitions between a free-flowing disordered and a spatially inhomogeneous jammed phase. Ordered structures are observed to drift, with a characteristic velocity, in the direction of the more mobile species.

PACS numbers: 64.60.Cn, 05.50.+q, 05.70.Fh, 05.70.Ln, 02.70.Rr

1. Introduction

Since their introduction, driven lattice gases have attracted much attention as some of the simplest systems for exploring non-equilibrium steady states [1, 2]. Motivated by the physics of fast ionic conductors [3], the earliest models consisted of a single species of 'charged' particles, diffusing on a periodic lattice, subject to the effects of both a thermal bath and an external (uniform, DC) 'electric' field. Driven by the field, the system settles into a state with non-trivial current. With no inter-particle interactions other than an excluded volume constraint, the *stationary state* distribution is trivial [4], and interesting behaviour is displayed only in *time-dependent* quantities. However, once interactions are introduced, then a variety of unexpected phenomena arise even in the steady state, such as long-range correlations at *all* temperatures [5].

A natural generalization is to study systems with two species, motivated by, e.g., fast ionic conductors with several mobile species [3]. Such systems have been used to model water droplets in microemulsions with distinct charges [6], gel electrophoresis [7, 8], vacancy mediated diffusion in binary alloys [9] and traffic flow [10]. Focusing on systems with two species carrying equal but opposite 'charge', we discovered remarkably complex steady states,

even for particles subjected only to the excluded volume constraint [11, 12]. For simplicity, the early studies employed only square lattices of $L \times L$, filled with equal numbers of 'positive' and 'negative' particles. The control parameters in this simple system are just E, the strength of the drive, and $\bar{m}$, the overall particle density (regardless of charge). By varying these parameters, we found that this model displays a phase transition [11], from a disordered state with homogeneous densities at small E or $\bar{m}$, to an ordered state with inhomogeneous densities. Moreover, this line in the E–$\bar{m}$ plane consists of a section with discontinuous transitions and another with continuous ones, which may be regarded as analogues of first- and second-order transitions in equilibrium systems. To understand these phenomena, it is sufficient to adopt a mean-field, continuum approach, based on hydrodynamic-like equations for the two conserved densities. A linear stability analysis around the homogeneous state allows us to predict the *existence* of transitions. Fortunately, we were able to find *analytic* solutions for both, homogeneous and inhomogeneous steady states [13], so that the presence of *both types* of transitions can be predicted. Subsequently, such models have been generalized to include rectangular lattices [12], non-neutral [14] or nearly filled [15] systems and 'charge exchange' dynamics [16] in one-dimensional [17] and quasi-one-dimensional [18, 19] cases. A dazzling array of surprising phenomena was discovered.

Here, we investigate a further generalization, namely, having species with different mobilities. Indeed, unless there are some underlying symmetry constraints, there is no reason to expect two different species of particles in typical physical systems to have identical mobilities. Using both Monte Carlo techniques and mean-field analyses, we find that, though the phase diagram appears to suffer little change, novel features arise in all regions of parameter space, even at not-so-subtle levels. In the next section, we present some details of how a differential mobility is implemented in simulations, followed by a discussion of our results. Section 3 is devoted to the continuum, mean-field theory and its predictions. We conclude with a summary of our findings and discuss some possible avenues for future investigations.

2. Model specification and simulation results

Following the first studies of biased diffusion of two species, square lattices of size $L \times L \equiv N$ are used. In most of our simulations, $L = 40$. We focus exclusively on neutral systems (i.e. $N_+ = N_-$) at various densities $\bar{m} \equiv (N_+ + N_-)/N$. A configuration of the system is specified by the set $\{\sigma_{x,y}\}$, where $\sigma_{x,y}$ assumes the values $0, \pm 1$ if the site (x, y) is empty or occupied by a positive (+) or negative (−) particle. Clearly, $\bar{m} = \sum_{x,y} \sigma_{x,y}^2 \big/ N$. The diffusive nature of the particles is modelled by allowing them to jump only to nearest-neighbour empty sites. After a particle and one of its neighbouring sites are selected, a particle–hole pair is always exchanged, unless it results in a particle jumping against the external 'electric' field. Chosen to point in the positive y axis, the field is parametrized by $\vec{E} = E\,\hat{y}$, so that its sole effect is to *lower* the probability of particle jumps against $\vec{E}$ to e^{-E}.

In contrast to previous studies, the two species are endowed with *different mobilities*, modelling say, trucks and cars on a road. Using the self-evident notation $\mu_\pm$ for the mobilities, we arbitrarily choose $\mu_+ \geqslant \mu_-$ and then focus on the ratio $\mu \equiv \mu_+/\mu_-$. To implement this ratio, we keep a list of the particles and their locations. In one Monte Carlo step (MCS), $\bar{m}N$ particles are chosen from the positive/negative list randomly with the frequency ratio of μ. In particular, by focusing on integer values of μ, we simply make μ attempts to move a positive particle for every attempt to move a negative one. By monitoring a few quantities, we found that there is little difference between sequential and random updating in species space, especially since the particle locations were randomly assigned at the beginning. After $\bar{m}N$ attempts, we increment the time by 1 MCS. Below, we will see that it is often convenient to

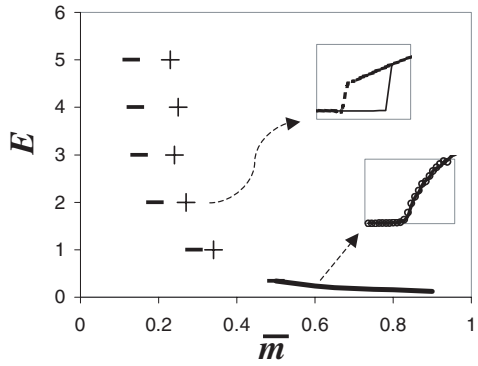

Figure 1. Phase diagram for mobility ratio of 30, with the system being homogeneous and 'jammed' in the lower-left and upper-right regions, respectively. The solid line marks continuous transitions. For discontinuous transitions, a pair of symbols (+/−) are used to denote the jumps in the order parameter when the filling fraction ($\bar{m}$) is increased/decreased. The absence/presence of hysteresis loops is illustrated by the insets, each containing data for sweeps in *both* directions (cf figure 2 for further explanations).

use the 'renormalized' MCS (1 RMCS being defined as $\mu + 1$ MCS), during which every slow particle would have had, on the average, one chance to move. Typically, 20K MCS or more are discarded before measurements are taken. In this study, we probe $\mu = 1, 3, 10, 30, 100$ and 300, though most of the data are collected for $\mu = 30$, being a compromise between exploring large differentials and dealing with finite computation times.

2.1. Continuous and discontinuous phase transitions

Similar to the $\mu = 1$ system, ours displays a transition from a disordered homogeneous to an ordered inhomogeneous state, the latter showing a macroscopic cluster with opposing particles locked in a 'jam.' To differentiate these phases, we monitor the first few *mass* structure factors, defined as

$$S_n \equiv \langle |\tilde{m}_n|^2 \rangle$$

where

$$\tilde{m}_n \equiv L^{-2} \sum_{x,y} \sigma^2_{x,y} \exp[2\pi \mathrm{i} n y / L]$$

with integer n, is the Fourier transform of the mass density profile across y. Here, $\langle \cdot \rangle$ denotes the average over 800 configurations, separated from one another by 100 MCS in a typical run of 80K MCS. We also measure the fluctuations in the S by monitoring the variances: $\langle [|\tilde{m}_n|^2 - S_n]^2 \rangle$. Both continuous and discontinuous transitions are observed, as illustrated by a phase diagram in the E–$\bar{m}$ plane for the $\mu = 30$ case (figure 1). The insets illustrate the nature of the transitions, in two typical parameter domains.

To provide further detail on how these lines are determined, we expand the insets of figure 1 into figures 2(*a*) and (*b*). Here, we plot the variations in S_1 as the system is swept *back and forth* across the transitions. For the continuous case (figure 2(*a*)), we show the result from a sweep in $E \in [0, 0.5]$ while $\bar{m}$ is held at 0.6. This direction of traversing the transition line is chosen because this line is almost parallel to the $\bar{m}$-axis in this region. Note that there are two sets of data points (×/−), representing the up/down sweeps from a single long run. This run is started with $E = 0$ in a random configuration at just over half filling ($\bar{m} = 0.6$).

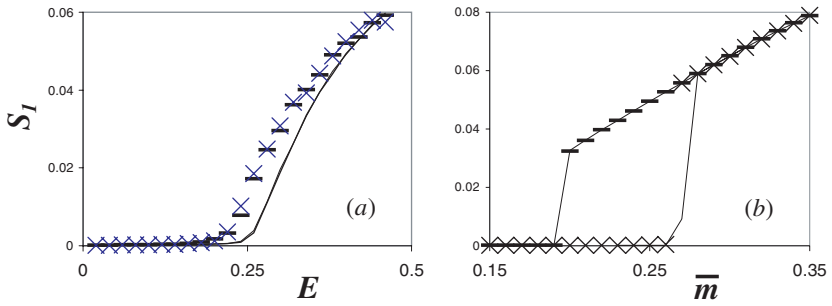

Figure 2. Plots of S_1 as the system are swept across the transitions. (*a*) E is increased ($\times$) and then decreased ($-$), with $\bar{m} = 0.6$ and $\mu = 30$. (*b*) $\bar{m}$ is increased ($\times$) and then decreased ($-$), with $E = 2$ and $\mu = 30$. For comparison, the $\mu = 1$ cases are shown as solid lines in both panels. With our statistics and accuracy, the effects of mobility differential are relatively minor.

Then, the first 20 K MCS are discarded, data gathered for the next 80 K MCS, E raised by 0.02, 20 K discarded and so on, until $E = 1.0$. Thereafter, the process is reversed, decreasing E until $E = 0$. The figure shows clearly that the transition is continuous with no sign of hysteresis. At the crude level of our investigations, the critical field is then identified through either the largest $\partial S_1/\partial E$ or the peak in the variance of S_1. The transition line is assembled by repeating such runs for $\bar{m} \in [0.5, 0.95]$ in steps of 0.05. For the discontinuous cases, which are more easily probed by sweeping in $\bar{m}$, we observe the typical hysteresis loops. The inset in figures 1 and 2(*b*) shows the case of $E = 2$. Again, the data represent a single long run, starting with $\bar{m} = 0.1$ in a random configuration, discarding the first 20 K MCS, gathering data for the next 80 K MCS as above, raising $\bar{m}$ by 0.01 and so on. These data points are represented by crosses ($\times$). After a run at $\bar{m} = 0.4$, we continue this process with decreasing $\bar{m}$ until $\bar{m} = 0.1$. This set of data is shown as minus signs ($-$). A hysteresis loop is clearly displayed, and the densities at the jumps are recorded to construct the points plotted in the main figure of figure 1. For comparison with the previous studies (i.e. the $\mu = 1$ case), we also show the results of such runs as solid lines in figures 2(*a*) and (*b*). As we see, there is little difference between the $\mu = 30$ and $\mu = 1$ results, leading us to conclude that, within the accuracy and statistics of our study, there is no significant dependence of the phase diagram on μ.

Before turning to the properties of the inhomogeneous state, let us remark that, of course, there *are* non-trivial effects due to $\mu > 1$, even in the disordered phase. Since one species is more mobile, there must be a difference between the average velocities, which in turn leads to a non-zero *mass* current even though $N_+ = N_-$. To verify this expectation, we measure the two currents, $J_\pm$, by simply keeping track of the number of $+/-$ particles which move up/down. Since $N_+ = N_-$ in our samples, the ratio of the average velocities is just $v_+/v_- = J_+/J_-$. With limited observations, our naive expectation:

$$J_+/J_- = \mu$$

turns out to be satisfied quite well. As the data in table 1 show, we have investigated only a few sample points, in both 'arms' of the disordered region (small E moderate $\bar{m}$, and vice versa).

Naturally, we expect other interesting properties associated with the disordered state; yet, these are generally quite subtle. For example, even in the $\mu = 1$ case, there are singular structure factors and long-range correlations [20]. For more prominent and fascinating features, we turn to the inhomogeneous state.

Table 1. Currents and their ratios for various regions in the homogeneous phase.

E	$\bar{m}$	μ	J_+/J_-	J_+	J_-
0.1	0.5	3	5.00	0.22	0.04
0.2	0.5	3	2.47	0.39	0.16
0.1	0.5	30	34.8	2.35	0.07
0.2	0.5	30	31.9	4.44	0.14
2.0	0.1	3	3.01	1.13	0.38
2.0	0.2	3	2.91	1.81	0.62
2.0	0.1	30	31.0	11.1	0.36
2.0	0.2	30	28.9	18.4	0.64

2.2. Drifting structures in the ordered state

Here, the density of particles is high enough so that they 'jam' into a macroscopic cluster. Consequently, the translational symmetry (in y) is spontaneously broken. In neutral systems with $\mu = 1$, the cluster performs an *unbiased* random walk, and, due to the symmetry under charge 'conjugation' ($+ \Leftrightarrow -$), its charge profile is purely antisymmetric. On the other hand, for charged systems (i.e. $N_+ \neq N_-$) this cluster drifts '*backwards*' (opposite to the average motion of the majority species)! Though counter-intuitive at first glance, this behaviour can be understood [14]. Simulating $\mu > 1$ systems here, we find the cluster to drift '*forwards*', i.e. in the direction of the more mobile species. Though this behaviour may seem less surprising, it is easy to advance a (wrong) heuristic argument to arrive at the opposite conclusion!

To characterize the drifting cluster more systematically, we carry out the following analysis. Since the runs are necessarily long, we focus only on neutral lattices with $\bar{m} = 0.36$, driven with $E = 1$. These parameters put us well in the ordered phase. To study the μ-dependence of the drift speed, we perform simulations with $\mu \in [2, 32]$ in steps of 2. For comparison with earlier studies, we also collect data for $\mu = 1$. Using a random configuration at the start, the usual first 20K MCS are discarded. To be sure that a macroscopic cluster is present, we first test the magnitude $|\tilde{m}_1|$ and proceed only when it is larger than 0.25 (cf, $|\tilde{m}_1| = 1/[L \sin(\pi/L)] \simeq 0.32$ for a fully ordered state). Assuming the centre of mass (CM) of the cluster is well characterized by the CM of the entire configuration, we measure the latter at intervals of 500 RMCS. Here, the CM of a particular configuration is defined simply by the phase in $\tilde{m}_1 = |\tilde{m}_1| \, \mathrm{e}^{\mathrm{i}\theta}$. Also, we find it more convenient to use the RMCS as a unit, since the time scale of the system as a whole is really set by the slow-moving particles. In the inset of figure 3, we show how θ depends on time for three μ. Clearly, the dominant behaviour is a steady drift. Fitting these data to $v_\theta t + \text{const}$, we extract the drift speed v_θ. Translating v_θ into a velocity, v, in units of lattice spacing per 1000 RMCS, we plot $v(\mu)$ in figure 3. Until we have some understanding of this quantity, we refrain from fitting it to a particular form. Instead, we just note that, interestingly, v seems to saturate at unity. Finally, we have computed the standard deviations from the linear fits naively and found that these are essentially independent of μ. Of course, since we believe the CMs to be performing (biased) random walks, we should expect these deviations to grow as $t^{1/2}$, from which diffusion coefficients can be extracted. Postponing such a detailed study to a later publication, what we may infer from our 'naive' computation is just that clusters associated with different μ execute random walks with the *same* diffusion constant but *different* biases.

Next, we consider the mass and charge profiles in the jammed state. For each configuration we measure both θ and

$$m(y) \equiv \frac{1}{L} \sum_x \sigma_{x,y}^2 \quad \text{and} \quad q(y) \equiv \frac{1}{L} \sum_x \sigma_{x,y}.$$

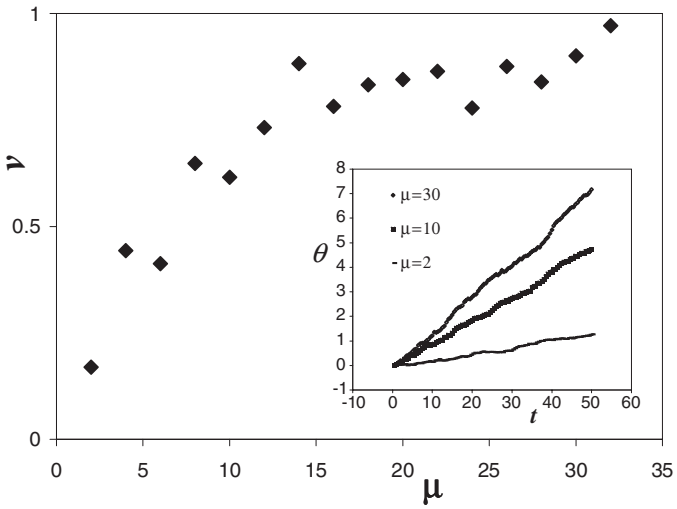

Figure 3. Drift speed as a function of μ. The inset shows the 'centre of mass' of the macroscopic cluster, as a function of time, for three values of μ.

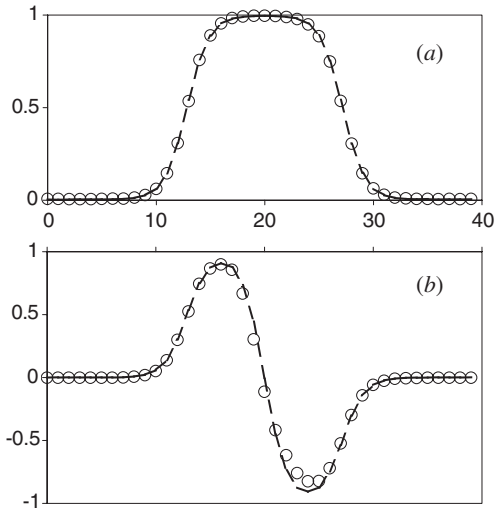

Figure 4. Mass (*a*) and charge (*b*) profiles in the ordered state. The dashed line and the open circles correspond to the $\mu = 1$ and $\mu = 30$ cases, respectively. Note that the charge profile for the latter is not purely antisymmetric about the CM ($L/2 = 20$).

Then we displace the y-dependent quantities according to $y \to u \equiv y - \theta L/2\pi + L/2$, so that the CM is located at $L/2 = 20$ for convenience. In this co-moving frame, we can now average over the run to produce the profiles: $\langle m(u)\rangle$ and $\langle q(u)\rangle$. Plotted in figure 4 are these profiles for the parameter set $(E, \bar{m}, \mu) = (1, 0.36, 30)$, and, for comparison with previous results, those for the $\mu = 1$ case as well. Even though the change in the mass profile appears almost imperceptible, there are actually some significant differences. For example, though the densities within (outside) the cluster differ by only about +0.003 (-0.003), this discrepancy translates into a *factor of two* for the densities far from the 'jam'. Until we have much better

statistics, it is unclear if we can attach much meaning to these subtle differences. The changes in the charge profile are more discernable. We may interpret these as an enhancement of the more mobile species' ability to penetrate into the block of the less mobile one.

3. Mean-field theory and comparisons

To develop a first-step understanding of the large scale phenomena shown above, we exploit the same mean-field approach which proved quite successful in the $\mu = 1$ case [11, 13]. In this approach, hydrodynamic-like equations of motion are postulated for the densities of the two species, $\rho_\pm(\vec{x}, t) \equiv \langle \sigma^2(\vec{x}, t) \pm \sigma(\vec{x}, t) \rangle / 2$:

$$\frac{\partial \rho_\pm}{\partial t} = -\vec{\nabla} \cdot \vec{J}_\pm$$

where $\vec{J}_\pm$ are the associated (density dependent) currents [11]. Here, we also treat the spatial co-ordinates as continuous variables, in general d dimensions: $\vec{x} = (x_1, \ldots, x_d \equiv y)$. To model differential mobility, we simply multiply the currents by $\mu_\pm$. Absorbing the average mobility into the time scale by defining

$$\mu_\pm \equiv (1 \pm \delta)$$

the continuum equations read

$$\frac{\partial \rho_\pm}{\partial t} = (1 \pm \delta)\vec{\nabla} \cdot [\phi \vec{\nabla} \rho_\pm - \rho_\pm \vec{\nabla} \phi \mp \rho_\pm \phi \mathcal{E} \hat{\mathbf{y}}] \tag{1}$$

where

$$\phi \equiv 1 - \rho_+ - \rho_-$$

is the hole density and $\mathcal{E}$ represents the coarse-grained electric field ($\mathcal{E} = 2 \tanh(E/2)$ at the most naive level). Of course, these equations can be re-expressed in terms of ϕ and the charge density

$$\psi \equiv \rho_+ - \rho_-$$

resulting in a form

$$\frac{\partial}{\partial t} \begin{pmatrix} \phi \\ \psi \end{pmatrix} = \begin{bmatrix} 1 & -\delta \\ -\delta & 1 \end{bmatrix} \begin{pmatrix} \nabla \cdot [\nabla \phi + \phi \psi \mathcal{E} \hat{\mathbf{y}}] \\ \nabla \cdot [\phi \nabla \psi - \psi \nabla \phi - \phi(1 - \phi) \mathcal{E} \hat{\mathbf{y}}] \end{pmatrix} \tag{2}$$

which easily reduces to the one studied previously [11, 13].

To find solutions to these equations, we must supply boundary conditions and constraints. For a hypercubic system of volume L^d, they are

$$\rho_\pm(\vec{x}, t) = \rho_\pm(\vec{x} + L\hat{x}_i, t) \qquad i = 1, 2, \ldots, d$$

and

$$\int \frac{\mathrm{d}\vec{x}}{L^d} \phi(\vec{x}, t) = 1 - \bar{m} \qquad \int \frac{\mathrm{d}\vec{x}}{L^d} \psi(\vec{x}, t) = 0.$$

We will discuss mainly steady states, i.e. density profiles which are time independent in a *co-moving* frame. From Monte Carlo results as well as previous experience with this model, we expect these profiles to obey translational invariance in the transverse directions in the whole parameter space. On the other hand, spontaneous breaking of translational invariance in y is manifest for the jammed state. Due to the drift, we will denote these profiles by $\phi(u)$ and $\psi(u)$, with $u = y - vt$.

3.1. Homogeneous states and linear stability analysis

Let us consider first the disordered phase, where the steady-state densities are homogeneous in both space and time, i.e.

$$\phi(\vec{x}, t) = 1 - \bar{m} \qquad \psi(\vec{x}, t) = 0.$$

Note that, unlike the $\mu = 1$ case, the mass current is no longer zero. The (average), denoted by $C\hat{y}$, is given through

$$C \equiv \hat{y} \cdot (\vec{J}_+ + \vec{J}_-) = \mu_+ \mathcal{E}(1 - \bar{m})\bar{m}/2 - \mu_- \mathcal{E}(1 - \bar{m})\bar{m}/2 = \delta \bar{m}(1 - \bar{m})\mathcal{E}.$$

With our normalization of time scales, the charge current is unchanged:

$$J \equiv \hat{y} \cdot (\vec{J}_+ - \vec{J}_-) = \bar{m}(1 - \bar{m})\mathcal{E}.$$

Some care is needed when direct comparisons of absolute currents with Monte Carlo data are made, since MCS and RMCS differ by a factor of $\mu + 1$. One test of this theory which is independent of such details is the ratio of current magnitudes

$$J_+/J_- = \mu.$$

As noted above, this prediction agrees well with our limited observations (apart from the first set, in which both currents are very small and noisy). Of course, our crude data should be regarded as merely the first step in a more refined study. That they are consistent with $J_+/J_- = \mu$ just confirms that this naive way of introducing mobility differentials is a reasonable starting point. Noting that the agreement is somewhat worse for high densities suggests the presence of subtle particle–particle correlations, which can only be uncovered by better statistics.

Beyond these trivial results, a linear stability analysis around this state leads us to the matrix

$$M = \begin{bmatrix} 1 & -\delta \\ -\delta & 1 \end{bmatrix} \begin{bmatrix} -k^2 & \mathrm{i}k_y\mathcal{E}(1 - \bar{m}) \\ \mathrm{i}k_y\mathcal{E}(2\bar{m} - 1) & -k^2(1 - \bar{m}) \end{bmatrix}$$

which is purposely written in a form to display the effects of $\delta > 0$. In contrast to the $\delta = 0$ case, the eigenvalues ($\lambda_{1,2}$) of this M are generically complex. Thus, we should examine their real parts to identify the stability limit. However, since M is real, it can be expressed as $|\lambda_1|^2 \operatorname{Re}\lambda_2/\operatorname{Re}\lambda_1$ (or $1 \Leftrightarrow 2$), so that $\det M = 0$ is still valid for identifying the stability limit. Since $\det M$ is modified by a simple factor of $(1 - \delta^2)$, we conclude that differential mobility has *no effect* on this line! In other words, the most unstable perturbation is still given by the lowest longitudinal mode:

$$k_y = 2\pi/L$$

and the instability occurs at [11]

$$(\mathcal{E}L/2\pi)^2(2\bar{m} - 1) = 1.$$

Of course, we cannot expect good quantitative comparisons with the phase boundaries from Monte Carlo simulations. For example, in the Ising model, mean-field analysis overestimates the critical temperature by nearly a factor of 2. Nevertheless, we are encouraged by one aspect of this prediction, namely, that differential mobility has no effect on the onset of the instability. This seems to be consistent with the observed phase boundaries being quite insensitive to μ.

For completeness, we give the explicit expressions for the eigenvalues:

$$\lambda_{1,2} = -k^2(1 - \bar{\rho}) - \delta\,\mathrm{i}k_y\mathcal{E}\bar{\rho} \pm \sqrt{R} \tag{3}$$

where

$$R = k^4[\bar{\rho}^2 + \delta^2(1-\bar{m})] - (k_y\mathcal{E})^2[(1-\delta^2)(2\bar{m}-1)(1-\bar{m}) + \delta^2\bar{\rho}^2] + 2\delta \mathrm{i}k^2 k_y \mathcal{E}\bar{\rho}(1-\bar{\rho}) \tag{4}$$

and $\bar{\rho} \equiv \bar{m}/2$. Their complex nature reflects drifts associated with the eigen-perturbations. Given that the species are mobile in different ways, such drifts are to be expected. In principle, it is possible to measure the decay and drift of small perturbations in simulations so that comparisons with these predictions can be made. In practice, however, such measurements would require better statistics and longer runs than those in this study.

3.2. Density profiles in inhomogeneous states

Turning to the more interesting ordered states, the most immediate question concerns the steady-state profiles. As observed in simulations and expected from symmetry considerations, these profiles are homogeneous in x but depend on y. In analogy to the $\mu = 1$ case, we seek non-trivial functions $\phi^*(y)$ and $\psi^*(y)$ which satisfy equation (2) in a steady state. However, it is clear from equation (1) that if non-trivial functions lead to zeros on the right-hand side with $\mu = 1$, then they also lead to zeros for any μ! The conclusion is that our mean-field theory admits inhomogeneous profiles which are (i) stationary (i.e. do not drift) and (ii) identical to those for $\mu = 1$. Of course, we may argue that this obvious discrepancy, when comparing with data, is a 'small' effect in absolute terms. However, our equations are non-linear and the existence of additional, drifting solutions cannot be ruled out. Unfortunately, we are unable so far, either to find drifting solutions (analytically or numerically), or to prove that our equations admit no such solutions. Nevertheless, for completeness, let us present the analysis which simplifies the problem to a single second order, non-linear, ordinary differential equation.

Following the techniques in [14], we assume the forms

$$\begin{pmatrix} \phi^*(\vec{x},t) \\ \psi^*(\vec{x},t) \end{pmatrix} = \begin{pmatrix} \phi^*(u) \\ \psi^*(u) \end{pmatrix}$$

where

$$u \equiv y - vt$$

with v being the drift velocity of the macroscopic cluster. Inserting these into equation (2), we obtain

$$-v\frac{\mathrm{d}}{\mathrm{d}u}\begin{pmatrix} \phi^* \\ \psi^* \end{pmatrix} = \frac{\mathrm{d}}{\mathrm{d}u}\begin{bmatrix} 1 & -\delta \\ -\delta & 1 \end{bmatrix}\begin{pmatrix} [(\mathrm{d}\phi^*/\mathrm{d}u) + \phi^*\psi^*\mathcal{E}] \\ [\phi^*(\mathrm{d}\psi^*/\mathrm{d}u) - \psi^*(\mathrm{d}\phi^*/\mathrm{d}u) - \phi^*(1-\phi^*)\mathcal{E}] \end{pmatrix}$$

which has the form of a vanishing total derivative. So, the first integrals are just constants which are identified with the two currents. As presented above, we denote the mass current C and the charge-current by J. Recognizing that the *hole* current must be $-C$, we obtain

$$\begin{pmatrix} C \\ -J \end{pmatrix} = v\begin{pmatrix} \phi^* \\ \psi^* \end{pmatrix} + \begin{bmatrix} 1 & -\delta \\ -\delta & 1 \end{bmatrix}\begin{pmatrix} [(\mathrm{d}\phi^*/\mathrm{d}u) + \phi^*\psi^*\mathcal{E}] \\ [\phi^*(\mathrm{d}\psi^*/\mathrm{d}u) - \psi^*(\mathrm{d}\phi^*/\mathrm{d}u) - \phi^*(1-\phi^*)\mathcal{E}] \end{pmatrix}. \tag{5}$$

To simplify these equations, we change variables, as in the $\delta = 0$ case, to

$$\chi \equiv 1/\phi^* \quad \text{and} \quad \omega \equiv \psi^*/\phi^*.$$

Then, we invert the matrix so that the first derivatives are decoupled:

$$\begin{pmatrix} -\mathrm{d}\chi/\mathrm{d}u + \omega\mathcal{E} \\ \mathrm{d}\omega/\mathrm{d}u - (\chi-1)\mathcal{E} \end{pmatrix} = \frac{-\chi}{1-\delta^2}\begin{bmatrix} 1 & \delta \\ \delta & 1 \end{bmatrix}\begin{pmatrix} -C\chi + v \\ J\chi + v\omega \end{pmatrix}.$$

Being first-order differential equations, their full solutions will require two more unknown integration constants. Together with C and J, there are four unknowns to be fixed, by the four constraint equations:

$$\chi(0) = \chi(L) \quad \text{and} \quad \omega(0) = \omega(L)$$

from periodic boundary conditions, as well as

$$\int_0^L \frac{1}{\chi} \mathrm{d}u = \int \phi^* = L(1 - \bar{m}) \quad \text{and} \quad \int \frac{\omega}{\chi} = \int \psi^* = 0$$

from the conservation laws. Further simplifications occur when we define C, J, v with appropriate factors of $\mathcal{E}, \delta$ and $1 - \delta^2$:

$$\frac{C}{1-\delta^2} \equiv \delta \mathcal{E} \tilde{C} \qquad \frac{J}{1-\delta^2} \equiv \mathcal{E} \tilde{J} \qquad \frac{v}{1-\delta^2} \equiv \delta \mathcal{E} \tilde{v}$$

so as to exploit the scaling of u to the variable $u\mathcal{E}$, and the symmetry of the system under $\delta \Leftrightarrow -\delta$ (with $\tilde{C}, \tilde{J}, \tilde{v}$ even in δ). Finally, denoting $\mathrm{d}/\mathrm{d}(u\mathcal{E})$ by prime ($'$), we arrive at

$$\chi' = \omega + \delta(\tilde{J} - \tilde{C})\chi^2 + \delta\tilde{v}\chi(1 + \delta\omega) \tag{6}$$

$$\omega' = (\chi - 1) - (\tilde{J} - \delta^2\tilde{C})\chi^2 - \delta\tilde{v}\chi(\delta + \omega). \tag{7}$$

One advantage of this form lies in that, in the limit $\delta \to 0$, it easily reduces to the previous case: $\chi'' = (\chi - 1) - \tilde{J}\chi^2$. The other is the clear separation of χ, ω into even/odd functions of δ. Note that, under this 'parity' operation, $u\mathcal{E}$ is odd.

As in the $\delta = 0$ case, the first equation can be trivially solved for ω and the resultant inserted into the second, leading us to a single (though quite complicated) equation for χ. As pointed out above, there exists at least *one* solution for any δ, corresponding to a stationary ($v = 0$) state and involving $\tilde{C} = \tilde{J}$ (i.e. $J = \delta C$).

Although we have not found non-trivial drifting solutions analytically, we are able to test the consistency of these equations against the measured profiles and v. For example, we can begin with equation (6) and integrate over u to get relationships between v and averages of the profiles. Indeed, there are infinitely many similar such relations, obtained from first multiplying this equation by functions of χ (or ϕ^*) before integration. To minimize possible large errors, we choose to consider two equations so that the averages involve no higher power of χ than unity. Specifically, we *divide* equation (6) by χ and χ^2 before integration. The results are

$$0 = \langle\psi\phi\rangle + \delta(\tilde{J} - \tilde{C}) + \delta\tilde{v}(1 - \bar{m}) \qquad 0 = \delta(\tilde{J} - \tilde{C})\langle\chi\rangle + \delta\tilde{v}(1 + \delta\langle\omega\rangle)$$

where the average is defined via

$$\langle\bullet\rangle \equiv \frac{1}{L}\int_0^L \bullet \, \mathrm{d}u.$$

Eliminating the unknown currents, we arrive at

$$\frac{v/\mathcal{E}}{1-\delta^2} = \frac{\langle\psi\phi\rangle\langle\chi\rangle}{1 - \langle\phi\rangle\langle\chi\rangle + \delta\langle\psi^*\chi\rangle}.$$

To compare with data, we retrace the rescaling of time and re-introduce the two mobilities, so that

$$v = \frac{2\mu_+\mu_-\langle\chi\rangle\langle\psi^*\phi^*\rangle\mathcal{E}}{(\mu_+ + \mu_-)[1 - (1 - \bar{m})\langle\chi\rangle] + (\mu_+ - \mu_-)\langle\psi^*\chi\rangle}.$$

Setting $\mu_+ = 30$ and $\mu_- = 1$ would correspond to using RMCS as a unit of time. Using the naive $\mathcal{E} = 2\tanh(E/2)$ with $E = 1$ and computing the appropriate averages from the

measured profiles (figure 4), this relation predicts $v \approx 0.004$. Being both of the right sign and order of magnitude, this is an encouraging result.

There is an alternative approach, based on a *discrete* version of a simple hopping model. Without delving into the details, we only state that it can be obtained as an approximation from the full master equation. By considering $\langle \sigma(\vec{x}, t) \rangle$ and ignoring all correlations, the result is a discrete equation for the average densities $\rho_\pm(\vec{x}, t)$. Focusing only on the y co-ordinate (i.e. averaging the densities over x), our starting point is

$$\rho_\pm(y, t+1) - \rho_\pm(y, t) = \frac{1}{4}\binom{\mu}{1}\{J_{\text{in}} - J_{\text{out}}\} \tag{8}$$

where the jumps into/out-of site y are given by

$$J_{\text{in}} \equiv \rho_\pm(y \mp 1, t)\phi(y, t) + \mathrm{e}^{-E}\rho_\pm(y \pm 1, t)\phi(y, t)$$
$$J_{\text{out}} \equiv \rho_\pm(y, t)\phi(y \pm 1, t) + \mathrm{e}^{-E}\rho_\pm(y, t)\phi(y \mp 1, t).$$

Here the time unit is a RMCS, while the factor $1/4$ accounts for half of jumps being transverse, so that each term in the J represents jumps with $1/4$ probability. Of course, periodic boundary conditions are imposed: $\rho_\pm(y, t) = \rho_\pm(y + L, t)$. For an inhomogeneous drifting steady state, we seek functions of the form $\rho_\pm(y, t) = \rho^*_\pm(u)$, so that we would write *naively*

$$\rho^*_\pm(u - v) - \rho^*_\pm(u) = \frac{1}{4}\binom{\mu}{1}\{\rho^*_\pm(u \mp 1)\phi^*(u) - \rho^*_\pm(u)\phi^*(u \pm 1)$$
$$+ \mathrm{e}^{-E}[\rho^*_\pm(u \pm 1)\phi^*(u) - \rho^*_\pm(u)\phi^*(u \mp 1)]\}.$$

Expecting v to be of the order of 10^{-3}, the first term on the left must be modified if we wish to apply this equation to data analysis. We believe a good approximation is to interpolate the left-hand side:

$$\rho^*_\pm(u - v) - \rho^*_\pm(u) \simeq v[\rho^*_\pm(u - 1) - \rho^*_\pm(u)].$$

Rearranging the result, we have

$$4v[\rho^*_\pm(u - 1) - \rho^*_\pm(u)] = \binom{\mu}{1}\{\mathrm{e}^{-E}\rho^*_\pm(u \pm 1)\phi^*(u) - \rho^*_\pm(u)\phi^*(u \pm 1)$$
$$+ \rho^*_\pm(u \mp 1)\phi^*(u) - \mathrm{e}^{-E}\rho^*_\pm(u)\phi^*(u \mp 1)\}$$

which can be 'integrated' once, as usual. The constants are just the steady-state currents ($J^*_\pm \equiv \hat{y} \cdot \vec{J}_\pm$), so that our basic equations read

$$4J^*_+ = \mu[\rho^*_+(u)\phi^*(u + 1) - \mathrm{e}^{-E}\rho^*_+(u + 1)\phi^*(u)] - 4v\rho^*_+(u) \tag{9}$$
$$4J^*_- = [\mathrm{e}^{-E}\rho^*_-(u)\phi^*(u + 1) - \rho^*_-(u + 1)\phi^*(u)] - 4v\rho^*_-(u). \tag{10}$$

In principle, these are recursive relations for the profiles and, imposing constraints $\left(\sum \rho^*_\pm = N_\pm\right)$, the unknown profiles and constants ($J^*_\pm$ and v) can be found. In practice, this method is not simple. Here, let us simply test these relations against the profiles from the data. By regarding e^{-E} also as an unknown, we can write four *linear* equations for these constants and see how good the agreement is. For simplicity, in a manner similar to the continuum study above, we choose to sum equations (9) and (10) for two equations. For the other pair, we first divide equations (9) and (10) by $\rho^*_\pm(u)$, respectively, and then perform the sum. The results are

$$\begin{bmatrix} J^*_+ \\ J^*_- \\ v \\ \mathrm{e}^{-E} \end{bmatrix} \simeq \begin{bmatrix} 0.99 \times 10^{-2} \\ -0.65 \times 10^{-3} \\ 0.63 \times 10^{-3} \\ 0.39 \end{bmatrix}.$$

Again, we are encouraged by how well this crude scheme functions, since the measured v is about 0.9×10^{-3} and $e^{-1} \simeq 0.37$. As for the currents, their small values are typical of jammed states. Though our data for them are too noisy for a meaningful comparison, we are quite satisfied by the relative magnitudes and signs.

4. Summary and outlook

We have reported simulation results and mean-field arguments for jamming transitions in a three-state lattice gas under non-equilibrium conditions. In our simple model, positive and negative particles diffuse on a lattice, subject to an excluded volume constraint and an external drive which biases their motion in opposite directions. Generalizing earlier studies of this model [11], we focus here on the effect of differential mobility, allowing one species to be more mobile than the other by a factor of μ. With equal numbers of the two species in the system, our key findings are as follows: The previously observed phase transition persists for the range $\mu \in [1, 300]$, i.e. a free-flowing state, for low densities ($\bar{m}$) and drive (E), giving way to a jammed phase at higher $\bar{m}$ and E. Moreover, there is little quantitative change to the $\bar{m}$–E phase diagram. Crossing the transition line at low $\bar{m}$ and high E, we observe hysteresis loops in the density structure factor, consistent with first-order transitions. Across the high $\bar{m}$ and low E portion of the line, the transitions are continuous. While the phase diagram is essentially unaffected by $\mu > 1$, both disordered and ordered phases exhibit a systematic drift, i.e. non-vanishing mass current. Focusing on ordered structures, we find that the cluster drifts in the direction of the more mobile species. According to the data, hole and charge density profiles depend in subtle ways on μ, and their drift velocity appears to saturate as μ increases. To shed more light on these findings, we present a mean-field theory, in the form of coupled, non-linear partial differential equations of motion for the hole and charge densities. Homogeneous solutions, corresponding to disordered phases, follow trivially from the conservation laws for the two particle numbers. A linear stability analysis demonstrates the presence of an instability, as the overall density increases. Unfortunately, we were not able to find inhomogeneous *drifting* solutions, so that we can only offer several consistency checks between equations and data, in order to build confidence in our theoretical description.

Many questions remain open for further study. First of all, a better understanding of the drift velocity would be desirable. Are there inhomogeneous solutions to our mean-field equations with non-trivial drift? If a proof of their absence can be established, then we should include noise terms (to promote the mean-field equations to Langevin equations) and study the effects of fluctuations and correlations. Perhaps these will renormalize the 'bare' coefficients in equation (1) so as to admit drifting structures. Such analysis, along with further simulations, should also settle the question whether the velocity continues to grow or approaches a saturation value as μ increases. In addition, the noise terms will allow us to investigate particle correlations and structure factors. As shown in preceding studies [20], these can be extremely interesting, even in the disordered phase. Going beyond *equal-time* structure factors, a study of *dynamic* correlations would provide considerable insight into currents and drifts. Finally, we note that, *at* the first-order line, we should find *coexisting* phases. Since the mass current is significant in the disordered region but quite small in the jammed region, these states will undoubtedly display a rich variety of behaviour.

Nearly all the simulations performed here are based on a 40×40 lattice. For fixed E, the observed transitions cannot possibly persist as the longitudinal size (L_y) goes to infinity. At the mean-field level, the inhomogeneous solutions effectively depend only on the product $\mathcal{E}L_y$. Thus, performing simulations with a range of E and L_y would be useful for establishing the presence of 'EL_y scaling' or proving its absence. In general, explorations of finite size effects

are clearly crucial before reliable conclusions on the nature of the phases and transitions can be drawn.

A natural expansion of parameter space is to allow for unequal numbers of the species. Such systems exhibit drifting structures even in the *absence* of differential mobility [14]. As a consequence, one might wonder whether it is possible to adjust these particle numbers and μ such that the jam becomes stationary. Viewed as traffic problems, involving cars and trucks at different densities and mobilities, the answers to these questions may shed some light on the essence of traffic jams.

Acknowledgments

We thank A Vasudevan for helpful discussions. This research was supported in part by a grant from the US National Science Foundation through the Division of Materials Research.

References

[1] Katz S, Lebowitz J L and Spohn H 1983 *Phys. Rev.* B **28** 1655
Katz S, Lebowitz J L and Spohn H 1984 *J. Stat. Phys.* **34** 497
[2] Schmittmann B and Zia R K P 1995 *Phase Transitions and Critical Phenomena* vol 17 ed C Domb and J L Lebowitz (New York: Academic)
[3] Chandra S 1981 *Superionic Solids. Principles and Applications* (Amsterdam: North Holland)
[4] Spitzer F 1970 *Adv. Math.* **5** 247
[5] Zhang M Q, Wang J S, Lebowitz J L and Vallès J L 1988 *J. Stat. Phys.* **52** 1461
Garrido P L, Lebowitz J L, Maes C and Spohn H 1990 *Phys. Rev.* A **42** 1954
[6] Aertsens M and Naudts J 1990 *J. Stat. Phys.* **62** 609
[7] Rubinstein M 1987 *Phys. Rev. Lett.* **59** 1946
Duke T A J 1989 *Phys. Rev. Lett.* **62** 2877
Schnidman Y 1991 *Mathematics in Industrial Problems IV* ed A Friedman (Berlin: Springer)
Widom B, Viovy J L and Desfontaines A D 1991 *J. Phys I (France)* **1** 1759
[8] Alon U and Mukamel D 1997 *Phys. Rev.* E **55** 1783
[9] Schmittmann B, Zia R K P and Triampo T 2000 *Braz. J. Phys.* **30** 139 *Preprint* cond-mat/9912135 and references therein
[10] Biham O, Middleton A A and Levine D 1992 *Phys. Rev.* A **46** R6128
Leung K-t 1994 *Phys. Rev. Lett.* **73** 2386
[11] Schmittmann B, Hwang K and Zia R K P 1992 *Europhys. Lett.* **19** 19
[12] Bassler K E, Schmittmann B and Zia R K P 1993 *Europhys. Lett.* **24** 115
[13] Vilfan I, Zia R K P and Schmittmann B 1994 *Phys. Rev. Lett.* **73** 2071
[14] Leung K-t and Zia R K P 1997 *Phys. Rev.* E **56** 308
[15] Schmittmann B and Thies M 2002 *Europhys. Lett.* **57** 178
[16] Korniss G, Schmittmann B and Zia R K P 1995 *Europhys. Lett.* **32** 49
Korniss G, Schmittmann B and Zia R K P 1997 *J. Stat. Phys.* **86** 721
[17] Arndt P F, Heinzel T and Rittenberg V 1999 *J. Stat. Phys.* **97** 1
Arndt P F and Rittenberg V 2002 *J. Stat. Phys.* **107** 989
[18] Korniss G, Schmittmann B and Zia R K P 1999 *Europhys. Lett.* **45** 431
[19] Mettetal J, Schmittmann B and Zia R K P 2002 *Europhys. Lett.* **58** 653
[20] Korniss G, Schmittmann B and Zia R K P 1997 *Physica* A **239** 111
Korniss G, Schmittmann B and Zia R K P 1997 *J. Phys.* A **30** 3837